TWELFTH EUROPEAN ROTORCRAFT FORUM

Paper No. 48

HELICOPTER MODELLING FOR PERFORMANCE CALCULATION

Karl Liese

Institute for Flight Mechanics
Technical University of Braunschweig

September 22-25, 1986

Garmisch-Partenkirchen
Federal Republic of Germany

Deutsche Gesellschaft für Luft- und Raumfahrt e.V. (DGLR)
Godesberger Allee 70, D-5300 Bonn 2, F.R.G.

HELICOPTER MODELLING FOR PERFORMANCE CALCULATION [+)]

Karl Liese
Institute for Flight Mechanics
Technical University of Braunschweig

Abstract

Methods for helicopter performance calculations are brought into line with the specific job in each case. Modern calculation techniques used in science and industry generally include analytical, empirical as well as experimental parts computing exact results within short time.
Essential parts of the helicopter physical model are studied such as downwash, blade-tiploss, hub-geometry, and blade-motions as well as blade and fuselage aerodynamics, and their influence on the power required and trim settings calculations are described.
The high variety of results, based on different modelling makes it possible to adapt existing calculation methods at hand for a new task or to bring about a new efficient method by combining suitable parts.

Notation

A	lift
a	hinge offset
C_A, C_a	lift coefficient
$C_{A\alpha}$	lift curve slope
C_F	thrust coefficient
C_m	momentum coefficient
C_P	*power coefficient*
C_W, C_w	drag coefficient
$C_{1..6}$	Mangler coefficients
F	thrust
I_β, I_ζ, I_ϑ	moments of inertia
K	trapezoidal factor
M	pitching moment
M_L, M_Z, M_G, M_F, M_D, M_{CO}	blade moments from airload, centrifugal force, weight, stiffness, damping, coriolis force
q	dynamic pressure
R, r, x	blade radius
S	rotor disk area
t	time
V	free stream velocity
W	drag
w_i	induced velocity
Z	number of blades
α	angle of incidence
α_{Ro}	angle of rotor disk due to free stream velocity
β	sideslip angle
β, $\dot\beta$, $\ddot\beta$	flapping angle, velocity, acceleration
β_K	precone angle (flapping)
ζ, $\dot\zeta$, $\ddot\zeta$	lagging angle, velocity, acceleration
ζ_K	precone angle (logging)
ϑ_o, ϑ_c, ϑ_s, ϑ_V	pitch angles, collective, cyclic and twist
λ	advance ratio
ρ	air density
Ω	rotor rotational speed

[+)] Work sponsored by the ministry of Research and Technology of the Federal Republic of Germany

1. Introduction

In the course of time, the knowledge of problems and interrelations typical for the helicopter problems as well as the possibilities of theoretical investigations and predictions have enormously improved. In this connection the possibility of using electronical computers certainly plays a decisive role.
Without doubt, a tendency towards increasingly complex mathematical model theories and calculation programs can be observed, however, the question should from time to time be considered whether the latest more complicated theories really produce best results and whether the approved less complicated procedures are really worn out. There is no doubt that the more simple physical models suffice for a variety of problems and even have advantages compared to the complex program systems /1/ which can be shown by comparing these calculation methods.
The power required is one of the most important factors in order to define the flight performance of a helicopter. Besides stability and thrust limits it restricts the flight envelope in terms of weight, hight, and velocity, the power required always having to be less than or the same as the power at hand. Thus, it is one of the most important tasks to investigate the power requirements by calculations in the design process as well as by measurements during flight testing of a helicopter that already exists.
Methods for helicopter trim and performance calculations do exist in different forms and complexity to cope with diverse requirements concerning accuracy and time of calculation in the respective stages of development. This way, simple models are used resulting from energy equations for power calculations in the early stage of development. In cases of calculating an already existing helicopter, procedures with extensive and complex models for the helicopter components are made use of. Obviously, there is a need for extensive calculation programs allowing investigations of all physical and geometrical influences possible, for instance for acoustic calculations or vibration investigations, however, it does not seem to be justified to make use of such models for less complicated tasks, such as performance calculations or investigations on stability and control, because they will merely have a higher absolute accuracy, are difficult to handle, and additionally are extremely involved.

2. Influence of Helicopter Modelling on Power Required

Modern methods for helicopter performance calculations applied in science and industry usually imply analytical, empirical, and experimental models that produce exact results at acceptable calculation expense. Procedures of this kind can as an example be seen in fig. 1 in a computer flow chart and are based on blade element momentum approaches for the rotor calculation. Apart from the numerical integration of the blade degrees of freedom, the numerical calculation of derivatives for the trim process is a decisive characteristic. Various models are possible and are used for part aspects such as rotorblade aerodynamics, downwash, tiploss, rotor geometry, blade degrees of freedom, fuselage aerodynamics, aerodynamics of tail surfaces and so on /2/.

2.1. Rotor Geometry and Blade Degrees of Freedom

It was only by introducing articulated rotor blades that the first successful helicopters could be developed. Therefore, rotors were built for a long time with mechanical joints allowing blade motions in three directions - the flapping and the lagging as well as the change of the angle of incidence, the feathering. The Puma rotor head in fig. 2 is an example.
Recently, the complexity of the rotor head is reduced by using elastic and flexible materials, fibre composites and elastomerics, making mechanical hinges superfluous and all motions are rendered possible by elastical bending or torsion, respectively. At the bottom of fig. 2 the MBB prototype rotor is shown.
All articulated and flexible rotor systems have a rather complicated geometry /3/. Modelling this means mathematical terms that are very difficult to survey on the one hand and an enormous calculation time on the other hand. Simplifications of the modelled rotor structure depend on the wanted accuracy of the results. In doing so, one should never forget the accuracy range of other part models.
The rotor model at hand is based on the geometrical dates of the BÖLKOW rotor system used in the helicopters MBB-Bo 105 and MBB/KHI-BK 117. The geometry of the rotor head is represented with the coordinate systems from fig. 3 and the respective matrix transformations. The complete model in fig. 4 serves as reference for comparative calculations with simplified models. The first simplification step refers to the omission of the angles of the inplane motion. In a second step, the flapping angles are also put to zero. An alternative model sums up the linearized angles of the flap and lag motion. In each of these methods, a vector of unity representing exemplarily a differential blade force or a local velocity vector is transformed for a typical rotor state from the middle of the rotor to the characteristic blade position with 75 % of the rotor radius.
From the wealth of results for different rotor states we see in fig. 5 the maximum deviations for individual vector components with the modelling being simplified in various ways. When ignoring the lagging angles, mistakes of up to 10 % are possible in the X and Y components in the blade system in unfavourable positions of the blade. Additionally ignoring the angles of the flapping motion results in maximum mistakes of up to 20 %. On the other hand, mistakes of only up to 2 % occur when linearizing the flap and lag angles and adding them to the respective coning angles.
Here, it should be pointed out once again that the mentioned percentages are only true for unfavourable blade positions, for example in the inner part of the blade or at very large angles of incidence and sideslip angles. As a rule, mistakes can neutralize one another when summed up during one rotor revolution. This is shown in fig. 6. The Z components, that means approximately the blade normal forces, lead to periodical differences during the blade revolution, but they cancel one another when calculating the average. This is however not always true for the other components. The average mistakes of all the models are smaller by a factor of 10. This way, the method with summarized and linearized angles leads to average mistakes of less than 0,5 %.
In the trim and performance calculation the various models cause differences in power that are located within the tolerances of the trim procedure. The effects on the calculated control angles are also so tiny that one can hardly interpret them. Thus, the enormous differences in the required calculation time are the reason for deciding on the most simple model in each case.

So far, the influence of the geometry on the transformation of vectors has been shown. In the following, the direct effects considering the blade motions flapping, lagging, feathering and blade torsion should be pointed out. This is shown in a diagram in fig. 7. The calculation expense is increased a great deal when calculating the blade motions within a trim and performance calculation.
Flap, lag, and torsion motions are at hand as non-linear differential equations and are solved by numerical integration. As the frequencies of blade torsion and elastic feathering are obviously higher than those of the flap and lag motion, considering them means integrating with clearly-reduced steps of rotor azimuth angle and thus an extremely longer calculation time. The stability of the other blade motions is also smaller compared to that of the flapping motion. This also leads to a high increase of calculation time in order to reach the equilibrium.
As most of the methods for performance calculations work with improved static aerodynamics, it must be doubted that models with higher order blade motions produce better results.
Different curves of the power required for flight states with a typical rotor load are shown in fig. 8. Only at high advance ratioes do the rotor degrees of freedom influence the power required. The rigid rotor, that means without any flapping or lagging motion, requires the highest level of power. The flapping rotor (flapping perpendicularily to the rigid disk) with various hinge offsets is shown in three curves. The smallest power requirements are calculated by the combined soft inplane flap and lag rotor model. A lot of curves from rotor models including the torsional mode and the flexible feathering mode are not shown because of a lack of survey in the diagram. All of them would have to be placed between the curves shown in fig. 8. Generally, the power required diverges at high advance ratioes, but it cannot be decided which curve is the right one. Differences between the curves do not result directly from the rotor modelling, including higher harmonics. What is more in this connection, different blade stiffness, hinge offsets, and phase displacement from combined blade modes effect significant changes in the body pitch attitude, leading to different forces and moments of the fuselage and empenage and in this way is incorporated directly into the power requirements. Higher harmonic blade motions also have less important consequences and are dependent on the kind of blade modelling. Influences of individual parameters such as stiffness and damping of a single mode is still liable to be investigated. Furthermore, sideforce equation of motion leads - considered or not considered - to different trim conditions, which influences the power requirement, too.

2.2. Downwash and Finite Number of Blades

The velocity state of the rotor blade and of the other body parts are only revealed exactly when considering the distribution of the induced velocity of the rotor. The lift-producing rotor blades can be regarded as wings of large extension in a harmonically-varying shear flow, the flow being subject to different interdependent influences of rotor blade, the vortex wake system and other helicopter components. The rotor blades induce a velocity in the downwash, thus deforming it. It is this distorted downwash system that induces in its turn a flow at the blades, changing the flow situation and the resulting aerodynamic forces at the blade. If almost all aspects of the vortex wake system are to be simulated, fairly complex calculations are effected /4, 5/ that are not suitable for trim and performance calculations due to their enormous calculation time.

A method that calculates the flight performance precisely enough is the determination of the average induced downwash velocity by means of the momentum theory, see fig. 9. Considering a constant inflow over the whole rotor disk that can be obtained from momentum approach is the most coarse and simple approximation for the calculation of the induced velocity. The rotor is regarded as an impulse disk that accelerates the inflowing air uniformily. This corresponds to the case of the rotor having an infinite number of blades. Despite the fact that the above assumptions are only true for axial states of flow, it is possible to similarly take axial flow components into consideration for the rotor in forward flight. An empirical factor which depends on the flight speed and attitude modifies the constant downwash distribution to a trapezoidal shape in the flight direction /6/.

Further applied methods for the calculation of the rotor downwash are various combined blade element momentum approaches /2, 7, 8/. Fig. 10 shows the model approach and the calculated distribution of a simple method that works with linear aerodynamics and blade element theory for axial rotor inflow. The varying state of flow during the revolution is ignored, as the dynamics of the blade motions is. Fig. 11 reveals the model approach and the distribution of an iterative method, taking into account non-linear aerodynamics, actual velocity including flapping motion and the current state of the feathering angle of the blade. Combined with an axial blade element momentum approach, an empirical approach for the transitory development of the induced velocity according to /7/ which is grounded on the results of /9/ leads to a distribution of downwash as shown in fig. 12.

The influence of the preceding rotor blades can be clearly seen. For reasons of comparison, the combined momentum potential theory of /10/ is used furtheron which can be seen in fig. 13. Regarding the free stream flow direction, the downwash distribution is symmetrical due to the potential approach. Compared with the vortex theories, all these methods need only little calculation time, so that they are suitable for trim and performance calculations.

As mentioned before, the momentum and potential models demand an infinite number of blades. In order to correct the occurring mistakes, an assumption for the compensation of dynamic pressure at the blade tip, the tiploss model, is taken into account. There are also different methods for this approach, shown in fig. 14. To a large extent, they are based on empirical interrelations developed by Prandtl and Glauert /11, 12/.

The two models on the top alter the induced downwash velocity, on the left changing the average and, on the right, altering only in the region of the blade tip. The two models below are changing the thrust correspondingly. On the left, the integration is only done as far as the reduced blade radius, on the right, the thrust is reduced only in the region of the blade tips.

As fig. 15 shows, there is an obvious range of results in power calculations with different models for downwash and tiploss. With the downwash model there are power differences of about 5 % in hover, of up to 20 % at medium advance ratioes and of up to 10 % at high speed. Besides the non-conformity of the downwash distribution, the average downwash velocity or the total inflow plays a decisive role. In the total velocity range, power differences of 4 to 5 % can be obtained with the tiploss models, deviations being dependent on the rotor load. The above calculations were done for an average value of $C_F = 0{,}004 \div 0{,}005$.

The collective pitch of the main rotor is a proportional result of the rotor load and the average downwash velocity. The differences in the collective pitch by comparing calculations almost correspond to the power differences. The influence of the model on the rotor collective pitch can accordingly be taken from the description of the power influence. The cyclic pitch, however, depends to a very large extent on the downwash distribution. This can be seen in fig. 16. The longitudinal cyclic pitch grows with increasing advance ratio, on the one hand for trimming differences in local thrust due to different velocity at the advancing and retreating blade, on the other hand compensating for the resulting pitching moments of the body. The longitudinal cyclic pitch angle is only insignificantly dependent on the choice of the downwash model. It is only the empirical local model that leads to triflingly higher sine pitch angles for larger advance ratioes, as when determining the local induced velocity it is not the actual flow but only the rotor rotational speed that is considered. The cosine share of the cyclic pitch angle, the lateral pitch, is determined by the irregularity of the rotor downwash along the longitudinal axis, and, to a minor extent, by the cross coupling of the rotor. The models GLOBAL, MANGLER, and the blade element momentum models show almost equal results. The larger cosine shares from the empirical model are a result of the larger increase of the downwash distribution along the X axis.

2.3. Rotorblade and Fuselage Aerodynamics

In order to determine the air loads at the blade section, profile characteristics are needed, that means the lift coefficient C_a and the drag coefficient C_w. Nowadays, aerodynamics are used that are taken from wind tunnel measurements with a real part of a blade. This is done to avoid influences of the Reynold number. To master the rotor states, the range of the angle of incidence must range over 360 degrees. Additionally, the influence of the Mach number must be known, see fig.17. During one revolution, the rotor blade is subject to quite different working conditions. At the advancing blade, the angles of incidence are low with high Mach numbers. At the retreating blade the angles of incidence are very high near the blade tip with average Mach numbers, and in the reversed flow field near the rotor hub the angles of incidence almost range over 360 degrees with Mach numbers being very low. When computing the air loads, most of the rotor models make only use of the normal and tangential velocity component, neglecting the effects of the radial flow. These consist of the mere effects of the sideslip which can be effected beyond the reversed flow field with angles up to +/- 90 degrees, furthermore of the effects of the radial flow at the rotor blade influenced by the centrifugal force. At the most important areas of the rotor, that is the outer and the blade tip region, the sideslip angle only has a minor extent. The consequence is that an omission has no significant effect.
Influenced by the centrifugal force, a radial flow in the boundary layer exists at the rotor blade. The centrifugal accelerations of the rotor blade reach values of 500 ÷ 1000 g. The resulting effects, mainly the influence of the stall characteristics, have not yet been examined sufficiently. A further deviation from the static lift coefficient and accordingly from the momentum coefficient normally asumed results from the lift hysteresis under the influence of a time dependent or periodical

change of the angle of incidence. In order to catch hold of this instationary effect at the blade section aerodynamics, which with the helicopter already appears during stationary flight, the time derivation of the angle of incidence or the pitch rate is needed besides the parameter Mach number for the actual blade profile, the frequency of the pitch rate respectively.
The general rotor calculation methods find only little favour of these instationary effects, one reason for this is that systematical profile measurements have not yet been sufficient. On the other hand this would mean additional expenditure /13/. Mostly, one resorts to correcting stationary aerodynamics with a so-called "dynamic factor", the "overshoot parameter", that means aerodynamics are used with an improved lift curve slope and lift coefficient.
The components of air loads and moments of the fuselage are estimated in rough calculations with empirical approximate solutions. For more exact performance calculations, a lot of measurements made with models in wind tunnels are usually taken as a basis. As regards the air load components of the fuselage it is the drag as well as lift and pitching moment that are interesting above all. For more detailed investigations it is also the factors side force and yaw moment that are significant. As an example, fig. 18 shows idealized body forces and moments as functions of the angle of incidence. Despite the fact that rather exact aerodynamics are considered, mistakes occur by calculating the average fuselage velocity. In this way, effects of interference, especially those affected by the rotor downwash, are not properly taken into account. The downwash distribution which is especially varying during forward flight can be considered by a cambering of the fuselage or by a fuselage finite element model.
Fig. 19 shows the influences of the important aerodynamic parameters of the blade profile C_{Amax} and C_{wo}. In the case that the profile drag is varied by 10 %, power differences of about 4 % are the result with a small rotor load and of about 3 % with a high load on the rotor. There are hardly differences in power required with a small or moderate rotor load when varying the maximum lift coefficient of the rotor blade. However, with a high load on the rotor, there can be important power differences at high advance ratioes.
It is known that lift and pitching moment of the fuselage are of minor importance, but as can be seen in fig. 20, a change in the drag of the fuselage means a change of power that increases with the forward flight speed. At medium advance ratioes, a drag decrease of 10 % means a saving of power of about 6 %. To a large extent this effect does not depend on the rotor load. The cyclic pitch angles are only insignificantly influenced by the conducted components variation.

3. Summary

The basis of power calculation is the blade element theory for propellers and rotors, modelling the rotor blade as a rigid beam with the flap and lag motion. By means of non-linear aerodynamics which depend on the Mach number, forces and moments at the blade are calculated. In doing so, the induced downwash velocity is usually taken into account from a model with a constant inflow or with trapezoidal inflow from Glauert when calculating the local velocity. In most cases, the influence of the fuselage is at hand in the form of wind tunnel data, model measurements being used scaled or corrected by Reynold number respectively. Simple non-linear models or lifting line approaches serve for the calculation of forces at the tail surfaces and wings. Purely

analytical methods have not yet been accomplished because the physics of important factors cannot be described exactly enough, such as blade tip aerodynamics, instationary effects, induced downwash distribution and aerodynamics of the fuselage. Moreover, the need of an extremely long calculation time of the mentioned models almost reaches the limits of performance of modern computers.
Modelling a complex system like the helicopter always works hand in hand with idealizing, neglect, approximation. No helicopter model, ever so good, can deliver satisfying results without empirical investigations. For a helicopter, design trim and performance calculations generally require high accuracy, and this, if possible, for the entire flight envelope of the helicopter. Calculation methods that meet these requirements are significantly characterized by empirical approaches of correction. It is the large variety of practicable methods for a physical model as well as the possibility of adapting the parameters in empirical and experimental approaches by which it is possible to adapt a calculation procedure that is already at hand to a new helicopter model, or to develop a new and more efficient method by skilfully combining suitable part models, respectively.

4. References

/1/ Gessow, A. — An Assessment of Current Helicopter Theory in Terms of Early Developments, in: Theoretical Basis of Helicopter Technology, Nov. 6-8, 1985, Nanjing, China

/2/ Stepniewski, W.Z.; Keys, C.N. — Rotary-Wing Aerodynamics, Dover Publications, Inc., New York, 1984

/3/ Johnson, W. — Recent Developments in the Dynamics of Advances Rotor Systems, AGARD Lecture Series No. 139, April 1985

/4/ Egolf, T.A.; Landgrebe, A.J. — Generalized Wake Geometry for a Helicopter Rotor in Forward Flight and Effect of Wake Deformation on Airloads, 40th Annual Form of the American Helicopter Society, Crystal City, Va., May 16-18, 1984

/5/ Miller, R.H. — Factors Influencing Rotor Aerodynamics in Hover and Forward Flight, 10th European Rotorcraft Forum, Den Haag 1984

/6/ Glauert, H. — A General Theory of the Autogyro, R + M No. 1111 (Ae. 285), London, 1926

/7/ Stricker, R.; Gradl, W. — Rotor Prediction with Different Downwash Models, 4th European Rotorcraft and Powered Lift Aircraft Forum, Stresa, Italy, Sept. 13-15, 1978

/8/ Azuma, A; Kawachi, K. — Local Momentum Theory and its Application to the Rotary Wing, AIAA 8th Fluid and Plasma Dynamics Conference 1975, AIAA Paper No. 75-865, 1975

/9/ Carpenter, J.P.; Fridovich, B. — Effect of a Rapid Black-Pitch Increase on the Thrust and Induced Velocity Response of a Full-Scale Helicopter Rotor, Naca TN 3044, 1953

/10/ Mangler, K.W.; Squire, H.B. — The Induced Velocity Field of a Rotor ARC-RM-2642, 1953

/11/ Prandtl, L. — Gesammelte Abhandlungen, 1. Teil, Springer Verlag Berlin 1935

/12/ Glauert, H. — Airplane Propellers, in: W.F. Durand: Aerodynamic Theory, Vol. IV, J. Springer Berlin 1935

/13/ Philippe, JJ. et al — A Survey of Recent Development in Helicopter Aerodynamics, AGARD-LS-139, April 1985

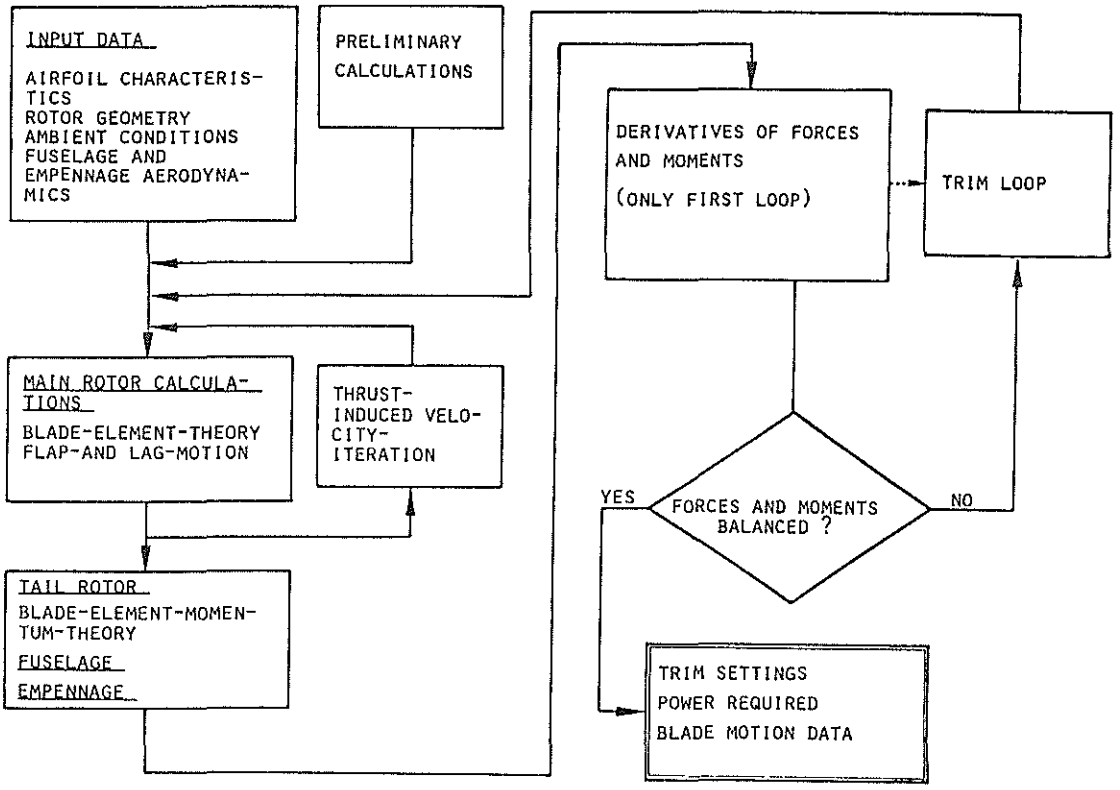

Figure 1. Performance Calculation Flow Chart

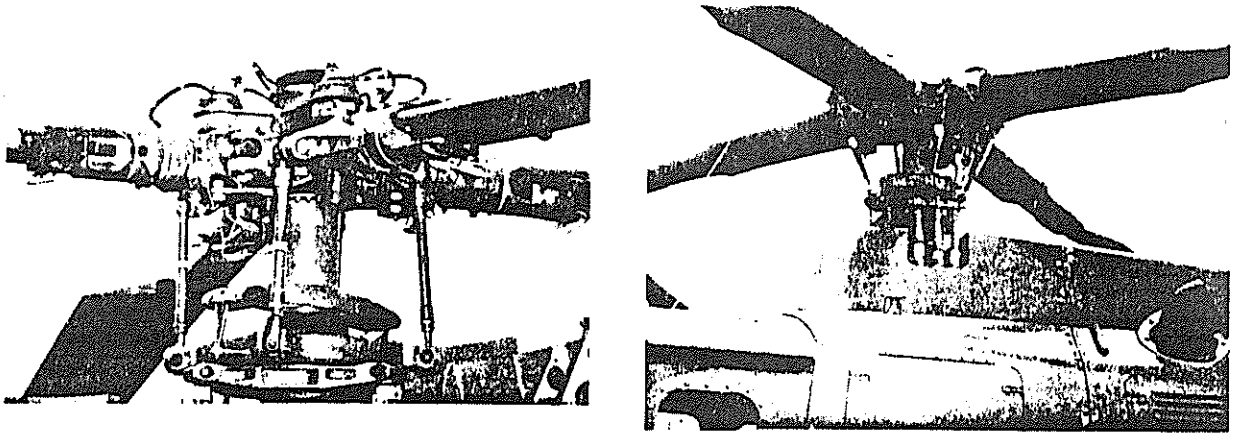

Figure 2. Rotorhead Systems

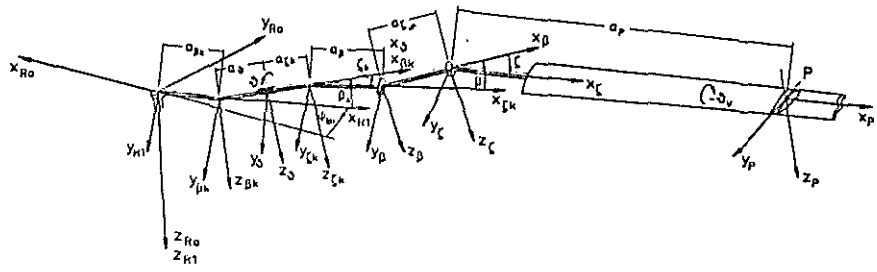

	Angles	Distances
Flap-coning	β_k	$a_{\beta k}$
Pitch	ϑ	a_ϑ
Lag-coning	ζ_k	$a_{\zeta k}$
Flapping	β	a_β
Lagging	ζ	a_ζ
Twist	ϑ_v	a_P

Figure 3. Geometry of the Main Rotor

```
MPRO(1,1) := - COS(THETABL)*COS(BETA)*COS(ZETA)*SIN(PSIBL)*SIN(
ZETAK) + COS(THETABL)*COS(PSIBL)*COS(ZETA)*SIN(BETA)*SIN(BETAK) -
COS(THETABL)*COS(ZETAK)*SIN(PSIBL)*SIN(ZETA) - COS(BETA)*COS(PSIBL)
*COS(ZETAK)*COS(BETAK)*COS(ZETA) - COS(BETA)*COS(PSIBL)*COS(ZETA)*
SIN(THETABL)*SIN(ZETAK)*SIN(BETAK) - COS(PSIBL)*COS(ZETAK)*SIN(
THETABL)*SIN(BETAK)*SIN(ZETA) + COS(PSIBL)*COS(BETAK)*SIN(ZETAK)*
SIN(ZETA) - COS(ZETA)*SIN(THETABL)*SIN(BETA)*SIN(PSIBL)$
MPRO(1,2) := - COS(THETABL)*COS(BETA)*COS(PSIBL)*COS(ZETA)*SIN(
ZETAK) - COS(THETABL)*COS(PSIBL)*COS(ZETAK)*SIN(ZETA) - COS(THETABL
)*COS(ZETA)*SIN(BETA)*SIN(PSIBL)*SIN(BETAK) + COS(BETA)*COS(ZETAK)*
COS(BETAK)*COS(ZETA)*SIN(PSIBL) + COS(BETA)*COS(ZETA)*SIN(THETABL)*
SIN(PSIBL)*SIN(ZETAK)*SIN(BETAK) - COS(PSIBL)*COS(ZETA)*SIN(THETABL
)*SIN(BETA) + COS(ZETAK)*SIN(THETABL)*SIN(PSIBL)*SIN(BETAK)*SIN(
ZETA) - COS(BETAK)*SIN(PSIBL)*SIN(ZETAK)*SIN(ZETA)$
MPRO(1,3) := - COS(THETABL)*COS(BETAK)*COS(ZETA)*SIN(BETA) - COS(
BETA)*COS(ZETAK)*COS(ZETA)*SIN(BETAK) + COS(BETA)*COS(BETAK)*COS(
ZETA)*SIN(THETABL)*SIN(ZETAK) + COS(ZETAK)*COS(BETAK)*SIN(THETABL)*
SIN(ZETA) + SIN(ZETAK)*SIN(BETAK)*SIN(ZETA)$
MPRO(2,1) := COS(THETAG)*COS(THETABL)*COS(BETA)*SIN(PSIBL)*SIN(
ZETAK)*SIN(ZETA) - COS(THETAG)*COS(THETABL)*COS(PSIBL)*SIN(BETA)*
SIN(BETAK)*SIN(ZETA) - COS(THETAG)*COS(THETABL)*COS(ZETAK)*COS(ZETA
)*SIN(PSIBL) + COS(THETAG)*COS(BETA)*COS(PSIBL)*COS(ZETAK)*COS(
BETAK)*SIN(ZETA) + COS(THETAG)*COS(BETA)*COS(PSIBL)*SIN(THETABL)*
SIN(ZETAK)*SIN(BETAK)*SIN(ZETA) - COS(THETAG)*COS(PSIBL)*COS(ZETAK)
*COS(ZETA)*SIN(THETABL)*SIN(BETAK) + COS(THETAG)*COS(PSIBL)*COS(
BETAK)*COS(ZETA)*SIN(ZETAK) + COS(THETAG)*SIN(THETABL)*SIN(BETA)*
SIN(PSIBL)*SIN(ZETA) - COS(THETABL)*COS(BETA)*COS(PSIBL)*SIN(THETAG
)*SIN(BETAK) - COS(THETABL)*SIN(THETAG)*SIN(BETA)*SIN(PSIBL)*SIN(
ZETAK) + COS(BETA)*SIN(THETAG)*SIN(THETABL)*SIN(PSIBL) - COS(PSIBL)
*COS(ZETAK)*COS(BETAK)*SIN(THETAG)*SIN(BETA) - COS(PSIBL)*SIN(
THETAG)*SIN(THETABL)*SIN(BETA)*SIN(ZETAK)*SIN(BETAK)$
MPRO(2,2) := COS(THETAG)*COS(THETABL)*COS(BETA)*COS(PSIBL)*SIN(
ZETAK)*SIN(ZETA) - COS(THETAG)*COS(THETABL)*COS(PSIBL)*COS(ZETAK)*
COS(ZETA) + COS(THETAG)*COS(THETABL)*SIN(BETA)*SIN(PSIBL)*SIN(BETAK
)*SIN(ZETA) - COS(THETAG)*COS(BETA)*COS(ZETAK)*COS(BETAK)*SIN(PSIBL
)*SIN(ZETA) - COS(THETAG)*COS(BETA)*SIN(THETABL)*SIN(PSIBL)*SIN(
ZETAK)*SIN(BETAK)*SIN(ZETA) + COS(THETAG)*COS(PSIBL)*SIN(THETABL)*
SIN(BETA)*SIN(ZETA) + COS(THETAG)*COS(ZETAK)*COS(ZETA)*SIN(THETABL)
*SIN(PSIBL)*SIN(BETAK) - COS(THETAG)*COS(BETAK)*COS(ZETA)*SIN(PSIBL
)*SIN(ZETAK) + COS(THETABL)*COS(BETA)*SIN(THETAG)*SIN(PSIBL)*SIN(
BETAK) - COS(THETABL)*COS(PSIBL)*SIN(THETAG)*SIN(BETA)*SIN(ZETAK)
 + COS(BETA)*COS(PSIBL)*SIN(THETAG)*SIN(THETABL) + COS(ZETAK)*COS(
BETAK)*SIN(THETAG)*SIN(BETA)*SIN(PSIBL) + SIN(THETAG)*SIN(THETABL)*
SIN(BETA)*SIN(PSIBL)*SIN(ZETAK)*SIN(BETAK)$
MPRO(2,3) := COS(THETAG)*COS(THETABL)*COS(BETAK)*SIN(BETA)*SIN(ZETA
) + COS(THETAG)*COS(BETA)*COS(ZETAK)*SIN(BETAK)*SIN(ZETA) - COS(
THETAG)*COS(BETA)*COS(BETAK)*SIN(THETABL)*SIN(ZETAK)*SIN(ZETA) +
COS(THETAG)*COS(ZETAK)*COS(BETAK)*COS(ZETA)*SIN(THETABL) + COS(
THETAG)*COS(ZETA)*SIN(ZETAK)*SIN(BETAK) + COS(THETABL)*COS(BETA)*
COS(BETAK)*SIN(THETAG) - COS(ZETAK)*SIN(THETAG)*SIN(BETA)*SIN(BETAK
) + COS(BETAK)*SIN(THETAG)*SIN(THETABL)*SIN(BETA)*SIN(ZETAK)$
MPRO(3,1) := - COS(THETAG)*COS(THETABL)*COS(BETA)*COS(PSIBL)*SIN(
BETAK) - COS(THETAG)*COS(THETABL)*SIN(BETA)*SIN(PSIBL)*SIN(ZETAK)
 + COS(THETAG)*COS(BETA)*SIN(THETABL)*SIN(PSIBL) - COS(THETAG)*COS(
PSIBL)*COS(ZETAK)*COS(BETAK)*SIN(BETA) - COS(THETAG)*COS(PSIBL)*SIN
(THETABL)*SIN(BETA)*SIN(ZETAK)*SIN(BETAK) - COS(THETABL)*COS(BETA)*
SIN(THETAG)*SIN(PSIBL)*SIN(ZETAK)*SIN(ZETA) + COS(THETABL)*COS(
PSIBL)*SIN(THETAG)*SIN(BETA)*SIN(ZETAK)*SIN(ZETA) + COS(THETABL)*
COS(ZETAK)*COS(ZETA)*SIN(THETAG)*SIN(PSIBL) - COS(BETA)*COS(PSIBL)*
COS(ZETAK)*COS(BETAK)*SIN(THETAG)*SIN(ZETA) - COS(BETA)*COS(PSIBL)*
SIN(THETAG)*SIN(THETABL)*SIN(BETAK)*SIN(ZETA) + COS(
PSIBL)*SIN(THETAG)*SIN(THETABL)*SIN(BETA)*SIN(BETAK)*SIN(ZETA) -
COS(PSIBL)*COS(BETAK)*COS(ZETA)*SIN(THETAG)*SIN(ZETAK) - SIN(THETAG
)*SIN(THETABL)*SIN(BETA)*SIN(PSIBL)*SIN(ZETA)$
MPRO(3,2) := COS(THETAG)*COS(THETABL)*COS(BETA)*SIN(PSIBL)*SIN(
BETAK) - COS(THETAG)*COS(THETABL)*COS(PSIBL)*SIN(BETA)*SIN(ZETAK)
 + COS(THETAG)*COS(BETA)*COS(PSIBL)*SIN(THETABL) + COS(THETAG)*COS(
ZETAK)*COS(BETAK)*SIN(BETA)*SIN(PSIBL) + COS(THETAG)*SIN(THETABL)*
SIN(BETA)*SIN(PSIBL)*SIN(ZETAK)*SIN(BETAK) - COS(THETABL)*COS(BETA)
*COS(PSIBL)*SIN(THETAG)*SIN(ZETAK)*SIN(ZETA) + COS(THETABL)*COS(
PSIBL)*COS(ZETAK)*COS(ZETA)*SIN(THETAG) - COS(THETABL)*SIN(THETAG)*
SIN(BETA)*SIN(PSIBL)*SIN(BETAK)*SIN(ZETA) + COS(BETA)*COS(ZETAK)*
COS(BETAK)*SIN(THETAG)*SIN(THETABL)*SIN(PSIBL)*SIN(BETAK)*SIN(ZETA) -
COS(ZETAK)*SIN(THETAG)*SIN(THETABL)*SIN(PSIBL)*SIN(BETAK) + COS(
BETAK)*COS(ZETA)*SIN(THETAG)*SIN(PSIBL)*SIN(ZETAK)$
MPRO(3,3) := COS(THETAG)*COS(THETABL)*COS(BETA)*COS(BETAK) - COS(
THETAG)*COS(ZETAK)*SIN(BETA)*SIN(ZETAK) + COS(THETAG)*COS(BETAK)*
SIN(THETABL)*SIN(BETA)*SIN(ZETAK) - COS(THETABL)*COS(BETAK)*SIN(
THETAG)*SIN(BETA)*SIN(ZETAK)*SIN(BETAK) + COS(BETA)*COS(ZETAK)*SIN(
BETAK)*SIN(ZETA) + COS(BETA)*COS(ZETAK)*SIN(THETAG)*SIN(THETABL)*
SIN(ZETAK)*SIN(ZETA) - COS(ZETAK)*COS(BETAK)*COS(ZETA)*SIN(THETAG)*
SIN(THETABL) - COS(ZETA)*SIN(THETAG)*SIN(ZETAK)*SIN(BETAK)$
```

Figure 4. Transformation from the Rotor-Center to the actual Blade-Point

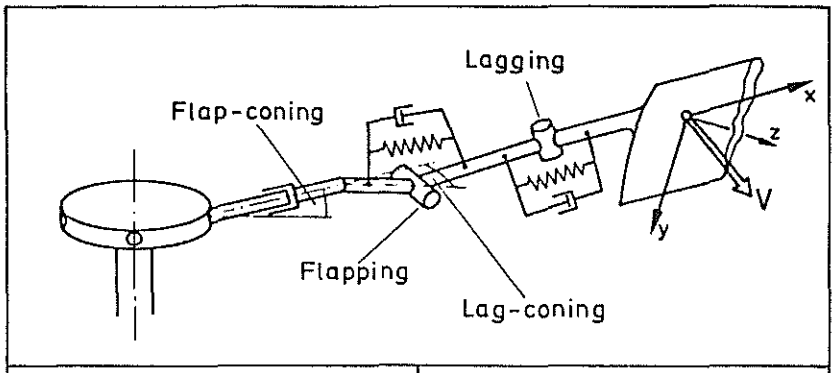

Simplification from Initial Model	Largest Fault from Vector-Transformation
Lagging: $\zeta_k = \zeta = 0$	<10 %
Lagging and Flapping: $\zeta_k = \zeta = \beta_k = \beta = 0$	<20 %
Linearized and combined Angles: $\sin x = x, \cos x = 1$ $\zeta_k + \zeta = \zeta^*$ $\beta_k + \beta = \beta^*$	< 2 %

Figure 5. Vector-Transformation with different Rotor-Models

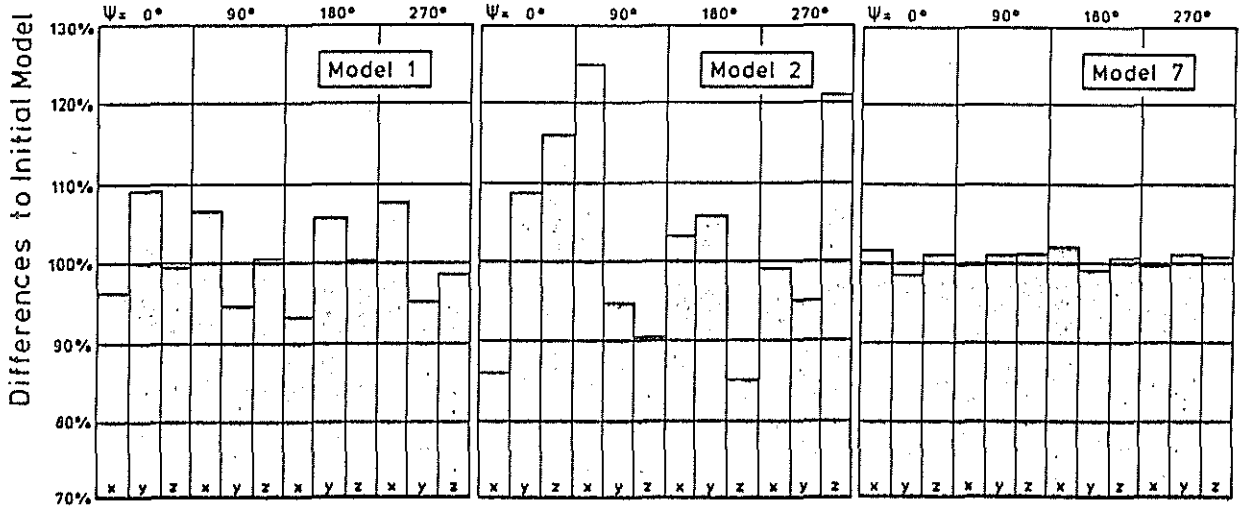

Figure 6. Vector-Transformation with different Rotor-Models (Components)

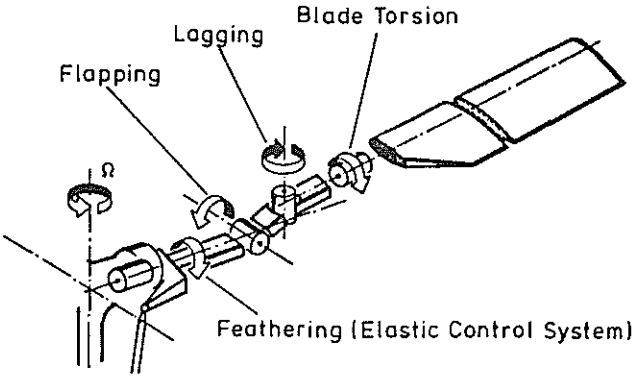

Flapping

$$\ddot{\beta} = \frac{-1}{I_\beta} \left[M_{L\beta} (\ldots,\beta,\dot{\beta},\zeta,\dot{\zeta},\vartheta,\dot{\vartheta}) + M_{Z\beta} + M_{G\beta} + M_{F\beta} + M_{D\beta} + M_{Co\beta} (\dot{\zeta}) \right]$$

Lagging

$$\ddot{\zeta} = \frac{-1}{I_\zeta} \left[M_{L\zeta} (\ldots,\beta,\dot{\beta},\zeta,\dot{\zeta},\vartheta,\dot{\vartheta}) + M_{Z\zeta} + M_{G\zeta} + M_{F\zeta} + M_{D\zeta} + M_{Co\zeta} (\dot{\beta}) \right]$$

Blade Torsion

$$\ddot{\vartheta} = \frac{-1}{I_\vartheta} \left[M_{L\vartheta} (\ldots,\beta,\dot{\beta},\zeta,\dot{\zeta},\vartheta,\dot{\vartheta}) + M_{F\vartheta} + M_{D\vartheta} \right]$$

Feathering (Elastic Control System)

$$\ddot{\vartheta}_E = \frac{-1}{I_{\vartheta E}(\beta,\zeta)} \left[M_{L\vartheta E} (\ldots,\beta,\dot{\beta},\zeta,\dot{\zeta},\vartheta,\dot{\vartheta}) + M_{F\vartheta E} + M_{D\vartheta E} \right]$$

Figure 7. Model of Blade Motions

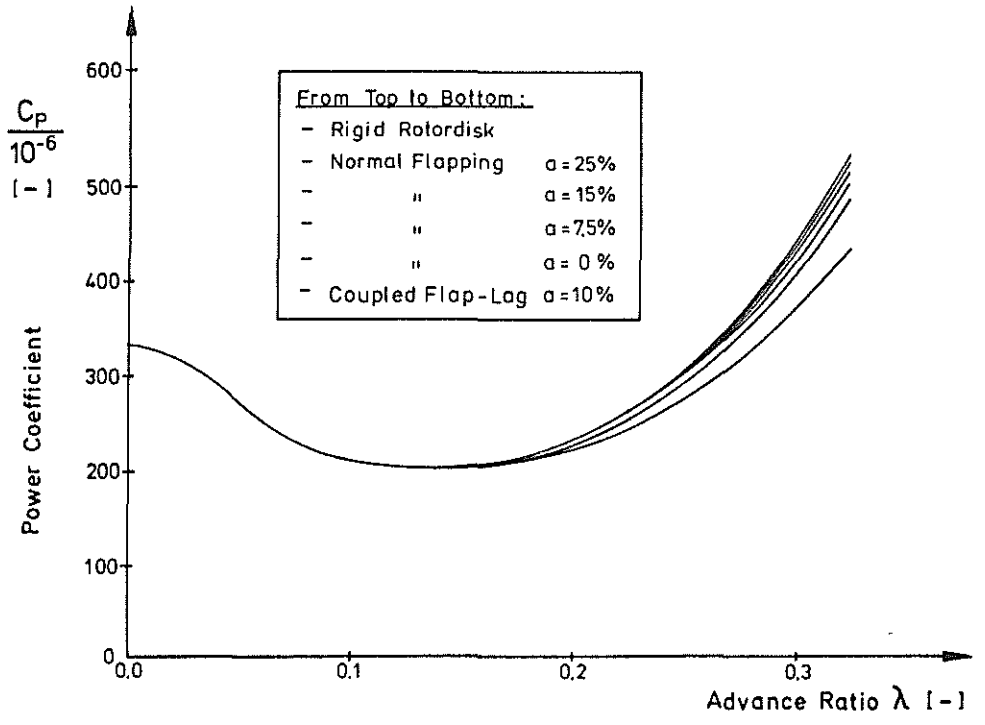

Figure 8. Performance Calculations with different Blade Models

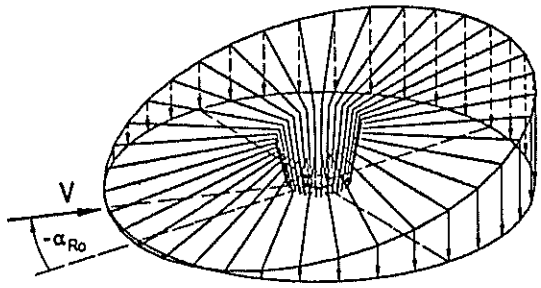

$$w_i(r,\psi) = w_{io}\,(1 + K\,\frac{r}{R}\cos\psi)$$

$$w_{io}^4 - 2\,V\sin\alpha_{Ro}\,w_{io}^3 + V^2\,w_{io}^2 = (\frac{F}{2\,\rho\,S})^2$$

$$K = \frac{4}{3}\,\frac{1}{1 + 1{,}2\left|\frac{-V\sin\alpha_{Ro} + w_{io}}{V\cos\alpha_{Ro}}\right|}$$

Figure 9. Induced Velocity from Momentum-Theory

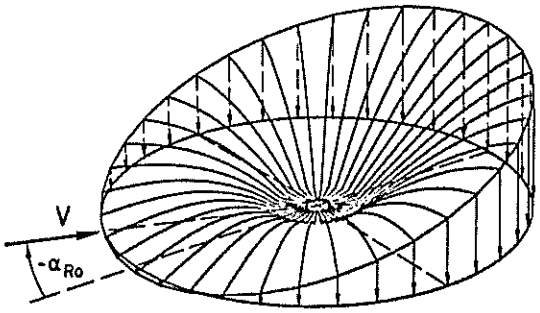

Momentum:

$$w_i^4 - 2\,V\sin\alpha_{Ro}\,w_i^3 + V^2 w_i^2 = (\frac{dF}{2\,\rho\,dS})^2$$

Blade Element:

$$dF = \frac{\rho}{2}\,(\Omega r)^2 \cdot C_{A\alpha}\,[\,\vartheta_o + \vartheta_V(r) - \frac{-V\sin\alpha_{Ro} + w_i}{\Omega\,r}\,]\cdot dS$$

Forward Flight Correction:

$$w_i(r,\psi) = w_i + w_{io}\cdot K\cdot\frac{r}{R}\cdot\cos\psi$$

Figure 10. Induced Velocity from Simple Blade-Element-Momentum-Model

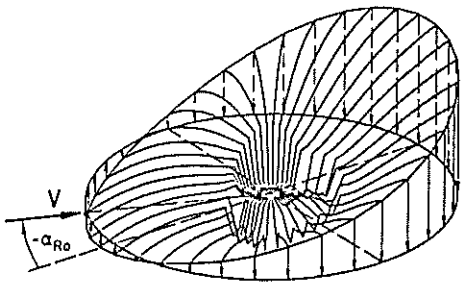

Momentum:

$$w_i^4 - 2\,V \sin\alpha_{Ro}\, w_i^3 + V^2 w_i^2 = \left(\frac{dF}{2\,\rho\,dS}\right)^2$$

Blade Element:

$$dF = \frac{c}{2}\, V_{Bl}(r,\psi)^2 \cdot C_A(r,\psi) \cdot dS$$

$$V_{Bl}(r,\psi) = \sqrt{[(\Omega + \dot\beta \cdot \sin\vartheta)\cdot r + V\cos\alpha_{Ro}\cdot\sin\psi]^2 + [\dot\beta\cos\vartheta\cdot r - V\sin\alpha_{Ro} + w_i]^2}$$

$$C_A(r,\psi) = C_{A\alpha}(\alpha,Ma)\cdot\left[\vartheta(r,\psi) - \frac{\dot\beta\cos\vartheta\, r - V\sin\alpha_{Ro} + w_i}{(\Omega + \dot\beta\sin\vartheta)\, r + V\cos\alpha_{Ro}\sin\psi}\right]$$

$$\vartheta(r,\psi) = \vartheta_o + \vartheta_s\cdot\sin\psi + \vartheta_c\cdot\cos\psi + \vartheta_v(r)$$

Forward Flight Correction:

$$w_i(r,\psi) = w_i + w_{io}\cdot K\cdot\frac{r}{R}\cdot\cos\psi$$

Figure 11. Induced Velocity from Iterative Blade-Element-Momentum-Theory

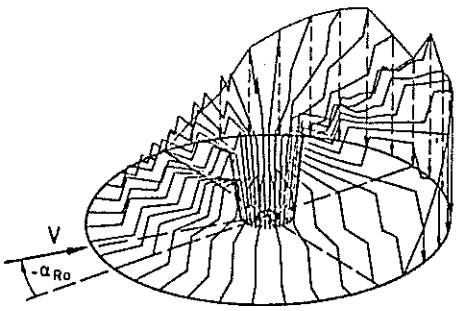

$$\begin{aligned} w_i(r,\psi) = {} & \Delta w_i(r_{i+1},\psi_{i+1})\ [1 - \tfrac{1}{2}\,(e^{-c_1\, t_{i+1}^2} + e^{-c_2\, t_{i+1}})] \\ & + \Delta w_i(r_{i+2},\psi_{i+2})\ [1 - \tfrac{1}{2}\,(e^{-c_1\, t_{i+2}^2} + e^{-c_2\, t_{i+2}})] \\ & + \Delta w_i(r_{i+3},\psi_{i+3})\ [1 - \tfrac{1}{2}\,(e^{-c_i\, t_{i+3}^2} + e^{-c_2\, t_{i+3}})] \\ & + \ \ldots \end{aligned}$$

w_i from Blade-Element-Theory

$$r_i\cdot\sin\psi_i = r_{i+1}\cdot\sin\psi_{i+1}$$

$$r_i\cdot\cos\psi_i - V\cdot\Delta t = r_{i+1}\cdot\cos\psi_{i+1}$$

$$\Omega\cdot\Delta t = \frac{2\pi}{z} + \psi_i - \psi_{i+1}$$

Figure 12. Empirical Downwash Model

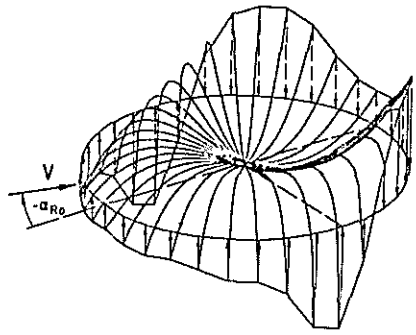

$$\frac{w_i(r,\psi)}{w_{io}} = 4\left[\frac{1}{2} C_o + \sum_{n=1}^{F} C_n(\mu,\alpha_{Ro}) \cdot \cos\left(n(\psi + 180°)\right)\right]$$

$$C_o = \frac{15}{8}\mu(1-\mu^2)$$

$$C_1 = -\frac{15}{256}\pi(5-9\mu^2)(1-\mu^2)^{\frac{1}{2}}\left(\frac{1-\sin\alpha_{Ro}}{1+\sin\alpha_{Ro}}\right)^{\frac{1}{2}}$$

$$C_2 = -\frac{1}{8}\left[(2+\mu)(9\mu^2-2)+9\mu\right]\left(\frac{1-\mu}{1+\mu}\right)\left(\frac{1-\sin\alpha_{Ro}}{1+\sin\alpha_{Ro}}\right)$$

$$C_3 = \frac{45\cdot\pi}{256}(1-\mu^2)^{\frac{3}{2}}\left(\frac{1-\sin\alpha_{Ro}}{1+\sin\alpha_{Ro}}\right)^{\frac{3}{2}}$$

$$C_4 = -\frac{1}{56}\left[(4+\mu)(9\mu^2+10)+45\mu\right]\left(\frac{1-\mu}{1+\mu}\right)^2\left(\frac{1-\sin\alpha_{Ro}}{1+\sin\alpha_{Ro}}\right)^2$$

$$C_6 = \frac{1}{504}\left[(6+\mu)(9\mu^2+30)+105\mu\right]\left(\frac{1-\mu}{1+\mu}\right)^3\left(\frac{1-\sin\alpha_{Ro}}{1+\sin\alpha_{Ro}}\right)^3$$

$$\mu = \sqrt{1-x^2}\ ,$$

Figure 13. Induced Velocity Field from Mangler + Squire

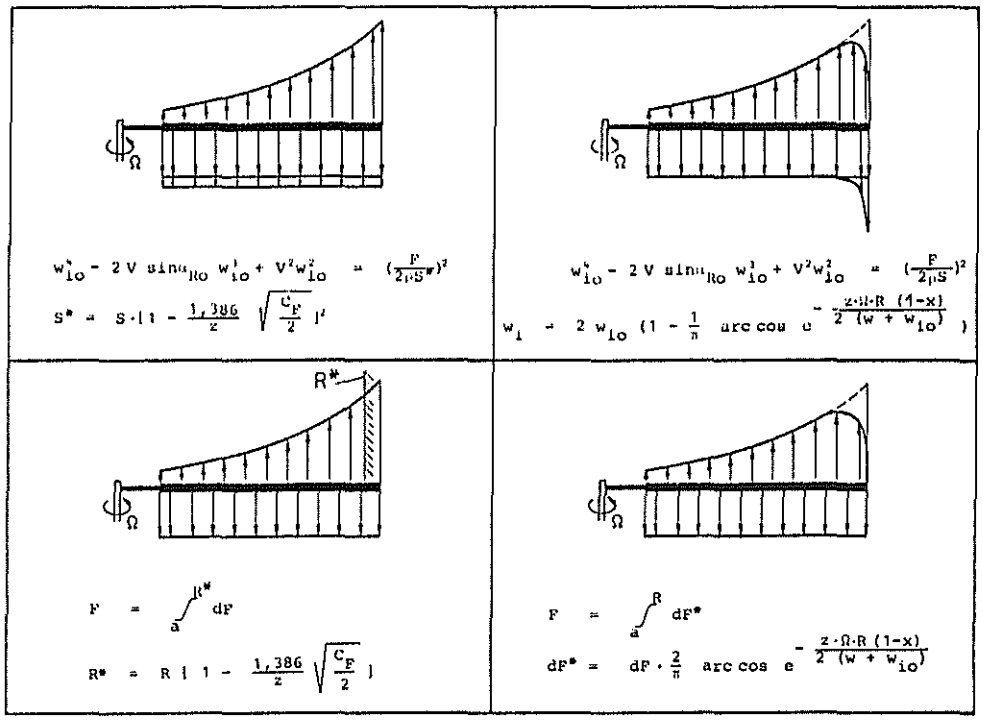

Figure 14. Different Tiploss-Models

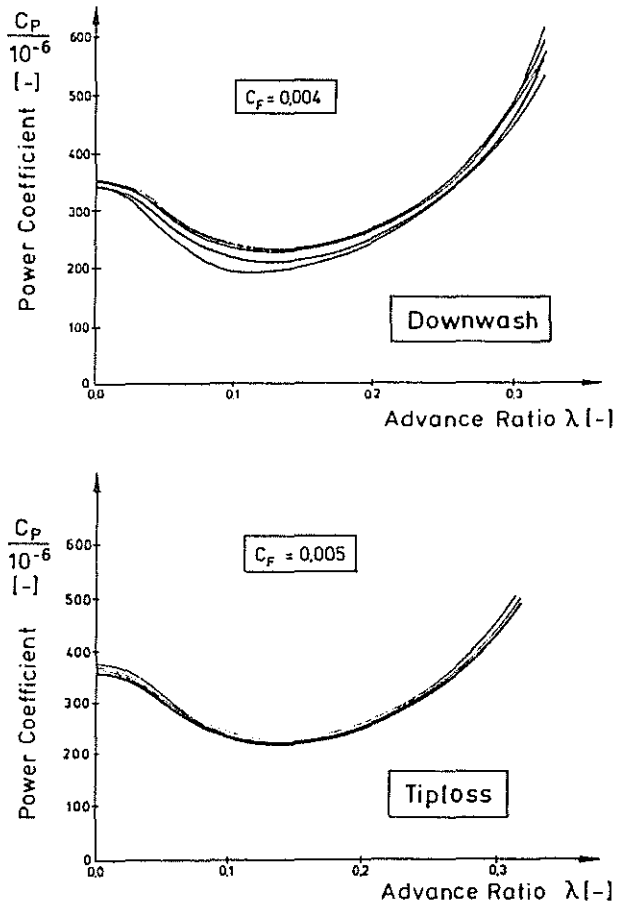

Figure 15. Performance Calculations with different Downwash and Tiploss Models

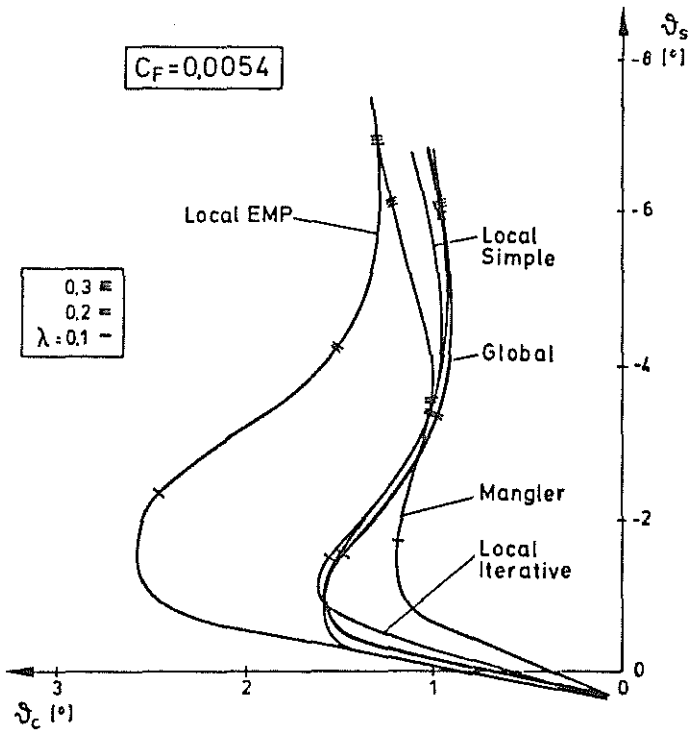

Figure 16. Cyclic Pitch Angles from different Downwash Models

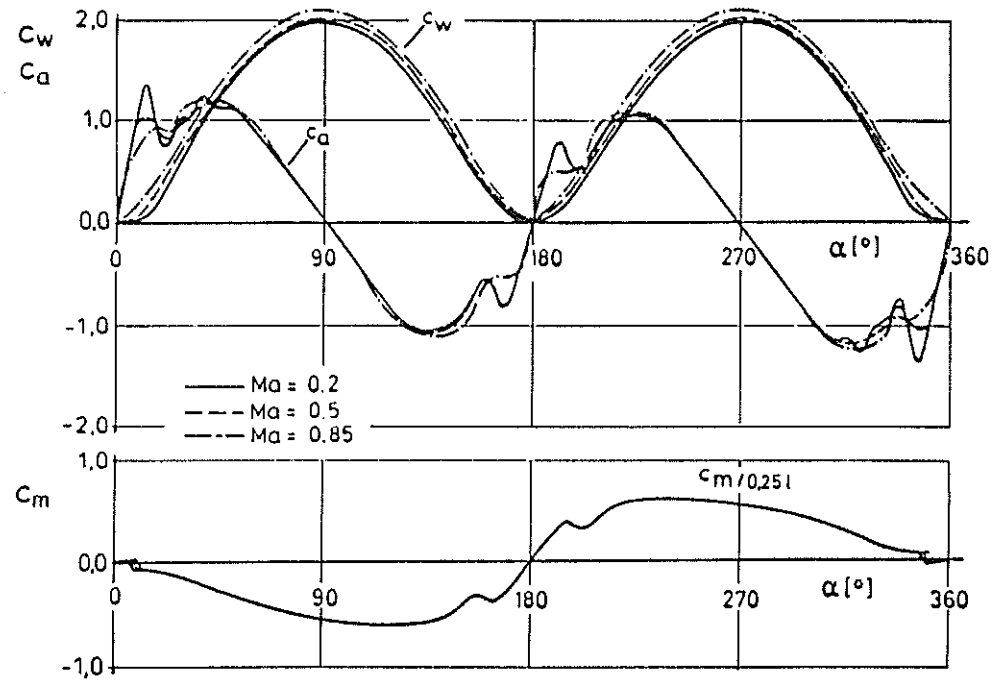

Figure 17. Airfoil section Drag, Lift and Moment

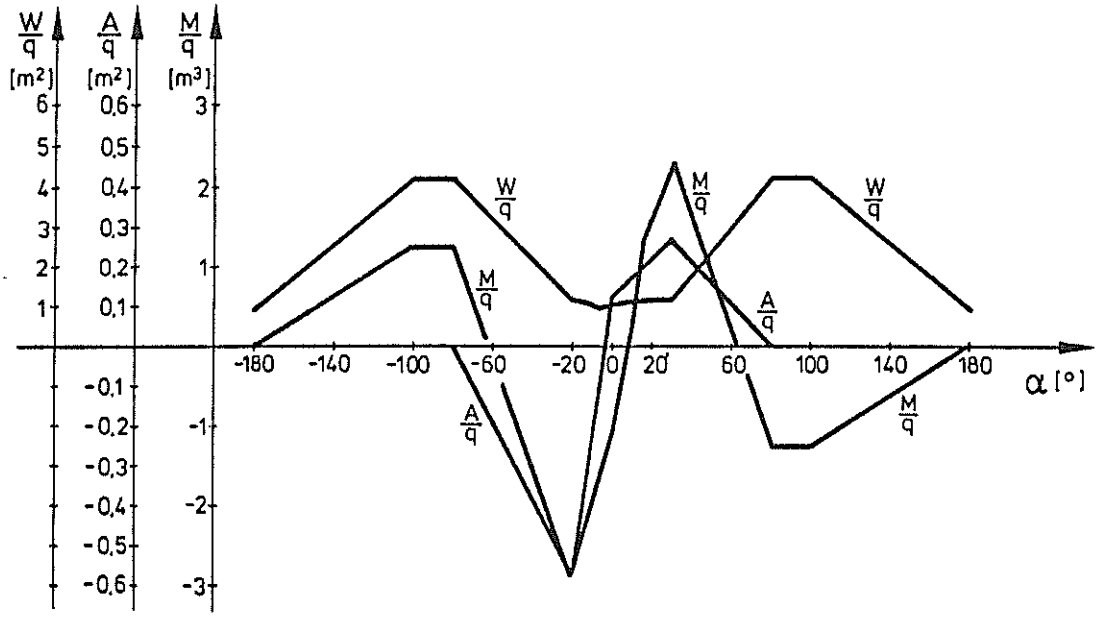

Figure 18. Fuselage-Drag, Lift and Moment

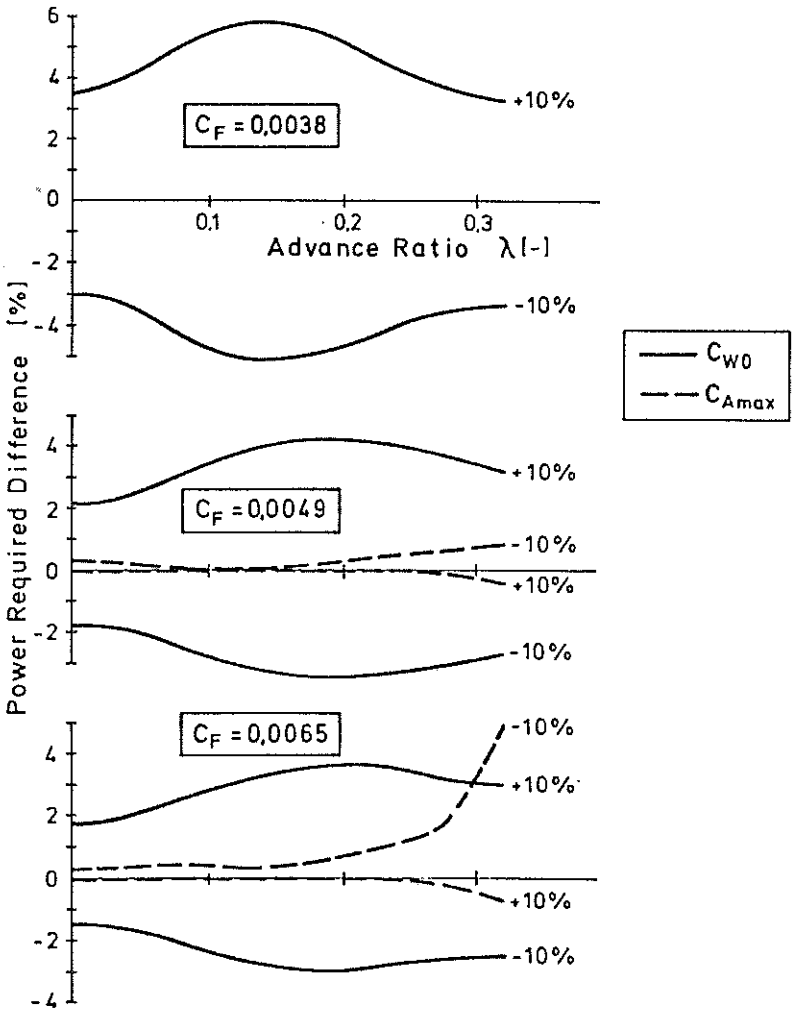

Figure 19. Influence of Blade Aerodynamic on Power Required

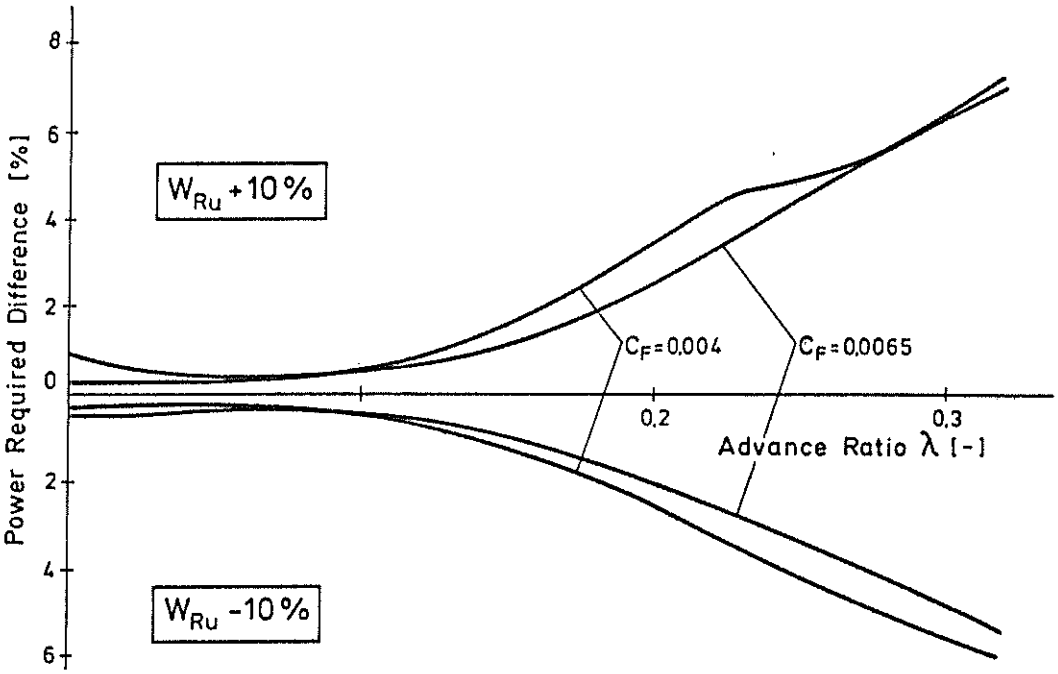

Figure 20. Influence of Fuselage-Drag on Power Required